Intrinsic polarization of elongated porous dust grains

Florian Kirchschlager [ORCID],[1]★ Gesa H.-M. Bertrang [ORCID][2] and Mario Flock [ORCID][2]

[1]*Department of Physics and Astronomy, University College London, Gower Street, London WC1E 6BT, UK*
[2]*Max Planck Institute for Astronomy, Königstuhl 17, D-69117 Heidelberg, Germany*

ABSTRACT

Observations of the Atacama Large Millimeter Array (ALMA) revealed recently polarized radiation of several protoplanetary discs in the (sub)millimetre wavelength range. Besides self-scattering of large particles, thermal emission by elongated grains is a potential source for the detected polarization signal. We calculate the wavelength dependent absorption and intrinsic polarization of spheroidally shaped, micrometre, and submillimetre sized dust grains using the discrete dipole approximation. In particular, we analyse the impact of dust grain porosity that appears to be present in discs when small grains coagulate to form larger aggregates. For the first time, our results show that (a) the intrinsic polarization decreases for increasing grain porosity and (b) the polarization orientation flips by 90 deg for certain ratios of wavelength to grain size. We present a new method to constrain grain porosity and the grain size in protoplanetary discs using multiwavelength polarization observations in the far-infrared to millimetre wavelengths. Finally, we find that moderate grain porosities ($\mathcal{P} \lesssim 0.7$) potentially explain the observed polarization fraction in the system HD 142527 while highly porous grains ($\mathcal{P} > 0.7$) fail unless the grain's axis ratio is extraordinarily large.

Key words: polarization – interplanetary medium – circumstellar matter – stars: pre-main-sequence – dust, extinction – infrared: planetary systems.

1 INTRODUCTION

Dust grains in protoplanetary discs are responsible for the absorption and scattering of both stellar and thermal radiation (in the optically thick regime). Besides the geometrical characteristics of these discs, dust grain properties such as their size, composition, and structure are the decisive elements for the optical appearance of the discs. Therefore, the disc's emitted and scattered light also carries information about the disc's building blocks – in total but also in polarized radiation.

Tamura et al. (1999) first detected polarized emission from T Tauri discs using SCUBA/JCMT. This polarization has been interpreted as thermal emission by magnetically aligned dust grains. Following detections of polarized signals from protoplanetary discs using SMA, CARMA, and VLA (Rao et al. 2014; Stephens et al. 2014; Segura-Cox et al. 2015), polarization observations at ∼ millimetre wavelengths have made a further leap forwards since high-resolved imaging of ALMA came available (Kataoka et al. 2016, 2017; Cox et al. 2018; Girart et al. 2018; Harris et al. 2018; Hull et al. 2018; Lee et al. 2018; Ohashi et al. 2018; Sadavoy et al. 2018; Dent et al. 2019; Harrison et al. 2019; Takahashi et al. 2019). The measured polarization signal is strongly influenced by the resolution of the observation, projection along the line of sight, dust properties, and (if applicable) alignment mechanisms of aspherical grains, and the interpretation of the polarized observations requires sophisticated models (Cho & Lazarian 2007; Bertrang, Flock & Wolf 2017; Bertrang & Wolf 2017).

Accordingly, the origin of the detected polarization signals is still highly debated. Besides dust scattering of anisotropic, thermal radiation of grains of size $\sim \lambda/(2\pi)$ (Kataoka et al. 2015), dichroic extinction and emission of aligned grains is supposed to be accountable for the polarized radiation (Cho & Lazarian 2007; Bertrang & Wolf 2017). When light passes an elongated grain, the component of the electric vector parallel and perpendicular to the short axis of the grain is differently absorbed that causes a net polarization, namely intrinsic (emission) polarization. Considering the huge number of dust grains in a disc, their individual polarization states would completely cancel out for disordered grains. However, grains can get aligned by several factors: the magnetic field (Lazarian & Hoang 2007), the radiation field (Lazarian & Hoang 2007; Tazaki, Lazarian & Nomura 2017), or mechanically (aerodynamically; Gold 1952).

So far, all studies considering polarization of elongated particles assumed solid dust grains (Draine & Weingartner 1996, 1997; Cho & Lazarian 2007; Lazarian & Hoang 2007). It is well known that dust grains grow by coagulation in protoplanetary discs, and as a result they might be porous. The occurrence of grain porosity is not only predicted by theoretical dust growth studies (e.g. Dominik & Tielens 1997; Ormel, Spaans & Tielens 2007) but also by laboratory

experiments (e.g. Blum & Wurm 2008; Kothe et al. 2013) as well as observations of circumstellar discs (e.g. Pinte et al. 2008; Milli et al. 2019). Moreover, the *Rosetta* orbiter detected fluffy grains in situ of the comet 67P/Churyumov–Gerasimenko (Fulle et al. 2015; Langevin et al. 2016; Mannel et al. 2016). Due to dust settling of more compact grains, porous grains are expected to occur cumulatively close to the disc surface, enhancing their contribution to the disc's optical appearance. Further, porosity has a huge impact on the grain's optical properties (e.g. Kirchschlager & Wolf 2013, 2014; Tazaki & Tanaka 2018; Ysard et al. 2018). Therefore, the study of elongated porous grains is promising to contribute to the comprehensive understanding of polarization by thermal emission.

In this work, we calculate the optical properties of spheroidally porous dust grains. In Section 2, we present the model for our dust grains and outline the calculation method. In Section 3, we discuss the wavelength-dependent absorption and intrinsic polarization of spheroidally porous grains, for single particles as well as for a grain size distribution. We discuss observed polarization fractions and introduce a procedure to derive the grain porosity from intrinsic polarization observations in Section 4 and give a summary in Section 5.

2 DUST MODEL AND METHODS

2.1 Elongated porous dust grains

In our study, the elongated porous dust grains have a spheroidally basic shape from which material is removed so that voids are formed. This model is comparable to that from Kirchschlager & Wolf (2013, 2014), where a spherically basic form is used. Here, we consider six spheroidally basic shapes with short semi-axis b and long semi-axis c: 3 prolate and 3 oblate shapes with $\frac{c}{b} \in \{1.1, 1.3, 1.5\}$, respectively. A prolate particle shape will be referred to as '1 − $\frac{c}{b}$ − 1' and an oblate shape as '$\frac{c}{b}$ − 1 − $\frac{c}{b}$'. The rotational axis of all spheroids is parallel to the y-axis in a Cartesian coordinate system ($x − y − z$; Fig. 1).

Porosity is the ratio of the vacuum volume to the total volume of the spheroidally grain,

$$\mathcal{P} = V_{\text{vacuum}}/V_{\text{total}} = 1 - V_{\text{solid}}/V_{\text{total}}. \tag{1}$$

Here, V_{total} is the volume of the encasing spheroid, $V_{\text{total}} = 4/3\pi b^2 c$ for prolate, and $V_{\text{total}} = 4/3\pi bc^2$ for oblate grains. The effective radius is the radius of a volume-equivalent solid sphere, $a_{\text{eff}} = \left(b^2 c(1 - \mathcal{P})\right)^{1/3}$ for prolate, and $a_{\text{eff}} = \left(bc^2(1 - \mathcal{P})\right)^{1/3}$ for oblate grains. We note that two grains composed of the same dust material and with the same effective radius a_{eff} have the same mass.

Our model enables the description of elongated porous dust grains by a low number of parameters ($a_{\text{eff}}, \frac{c}{b}, \mathcal{P}$), while the definition of the porosity is still accurate. Contrary, the porosity definition in many other studies suffers by the fact that the total volume is that of a sphere encasing the dust particle, even for highly aspherical grains such as BCCA aggregates (e.g. Kataoka et al. 2014; Tazaki & Tanaka 2018). When the encompassing body is a sphere, the porosity is artificially high; for example, a solid but prolate dust grain with $\frac{c}{b} = 10$ (compact needle) would have a porosity of ~ 99 per cent. In contrast, our definition of porosity gives the correct value of $\mathcal{P} = 0$ and an overestimation of the porosity is excluded.
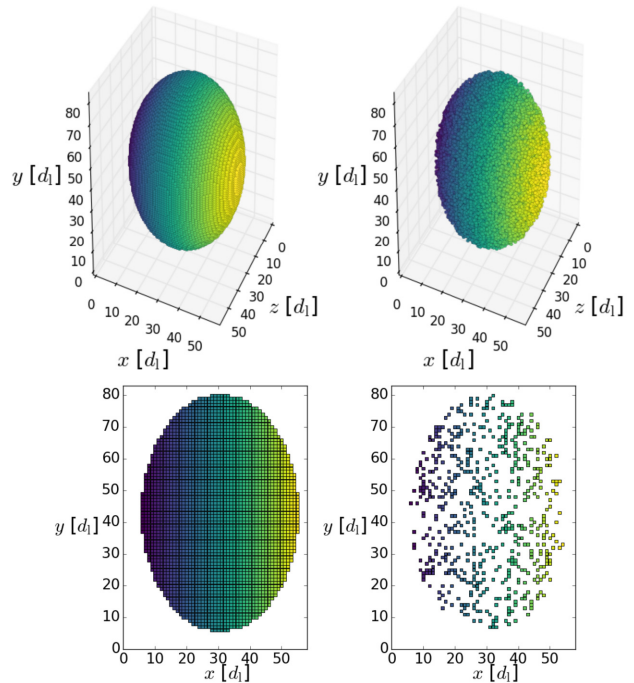

Figure 1. Morphology of elongated dust grains (1-1.5-1). *Top:* A compact grain composed of 96 912 cubic subvolumes (*left*; $\mathcal{P} = 0.0$) and a porous grain of 19 382 cubic subvolumes (*right*; $\mathcal{P} = 0.8$). *Bottom:* Single-layer of cubic dipoles through the centre of the compact and porous elongated grain, respectively. The colour scale is only for illustration purposes.

2.2 Calculation method

To calculate the optical properties of irregular-shaped particles, we use the code DDSCAT[1] (version 7.3; Draine & Flatau 1994, 2010) that is based on the theory of discrete dipole approximation (DDA; Purcell & Pennypacker 1973). The three-dimensional particle shape is replaced by a corresponding spatial distribution of N discrete dipoles on a cubic grid and the optical properties are then calculated for this dipole distribution. The DDSCAT is well tested and is applicable for most particle shapes and structures. However, the applicability is constrained by an upper limit of the ratio of grain size a_{eff} to wavelength λ (see e.g. Draine & Goodman 1993; Draine & Flatau 1994; Draine 2000). For porous dust grains, this condition is given by (Kirchschlager & Wolf 2013)

$$\frac{a_{\text{eff}}}{\lambda} \lesssim 0.1 \frac{N^{1/3}}{|n(\lambda)|}, \tag{2}$$

where $n(\lambda)$ is the wavelength-dependent complex refractive index. The lowest number of dipoles used in this study is $N = 19382$, and with $|n(\lambda)| \sim 3$ (for astronomical silicate at $\lambda = 100\,\mu\text{m}$)[2] follows: $\lambda \gtrsim a_{\text{eff}}$. As the ratio of the effective radius a_{eff} to wavelength λ increases, so does the necessary computation time. For the 1 and 10 μm grains, the optical properties can be calculated in less than 2.5 core hours using a 2.70 GHz central processing unit (CPU), whereas the calculations for a 100 μm grain took approximately 7.5 d.

---

[1] https://www.astro.princeton.edu/draine/DDSCAT.7.3.html
[2] For carbon and ice is $|n(\lambda)| \sim 1.8$ at $\lambda = 100\,\mu\text{m}$, and it follows $\lambda \gtrsim 0.7 a_{\text{eff}}$.
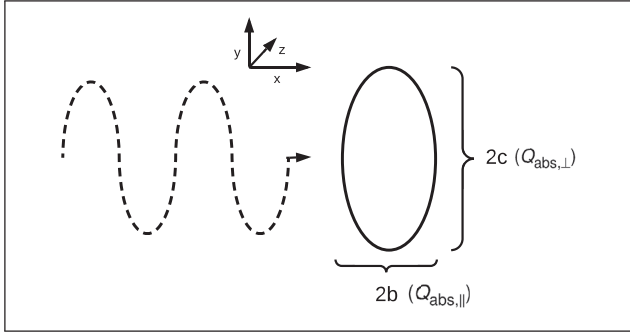
Figure 2. Sketch of the irradiation of an elongated particle.

2.3 Porous structure

The method to generate the porous dust grains is described in detail in Kirchschlager & Wolf (2013) and briefly summarized here: N' dipoles are arranged on a cubic lattice with lattice constant d_l, forming the shape of a compact spheroid with semi-axis b and c and a total volume of $N'(d_l/2)^3 = 4/3\pi a_{eff}^3 (1 - \mathcal{P})^{-1}$. In order to create a porous grain of porosity $\mathcal{P}$, $\mathcal{P}N'$ dipoles are randomly removed. Then the remaining dipole arrangement of $N = (1 - \mathcal{P})N'$ dipoles forms the elongated porous dust grain (Fig. 1). Each dipole represents a cubic subvolume d_l^3 of the dust material, while a removed dipole represents a cubic void of the same size. The large number of dipoles ($\sim 10^5$–10^6) ensures a statistical distribution of the voids within the grains and a good approximation of the spheroidally basic shape.

Using this method, the dipole configurations of six particle shapes and nine porosities ($\mathcal{P} = 0.0 - 0.8$; in steps of 0.1) are generated. We calculate the optical properties for each of the 54 (=6 × 9) dipole configurations for the grain sizes $a_{eff} = 1$, 10, and 100 µm in the wavelength range $\lambda \in [100\,\mu m, 2000\,\mu m]$ for the case that the radiation is propagating parallel to the x-direction (Fig. 2). We consider grains of three different dust materials: astronomical silicate (Draine 2003a,b), carbon (Jäger, Mutschke & Henning 1998), and ice (Warren 1984; Reinert et al. 2015). We have seen in Section 2.2 that the chosen number of dipoles and dust materials is sufficient to calculate the optical properties for dust grains up to $a_{eff} = 100\,\mu m$ for the shortest wavelengths $\lambda = 100\,\mu m$.

3 RESULTS

3.1 Polarized emission of single dust grains

When the rotational axis of the elongated grain is parallel to the y-direction and the photons travel parallel to x-direction, photons 'see' an ellipsoidally geometric cross-section of the grain defined by the short and long semi-axis, b and c, respectively. The electric field parallel to the short axis sees a smaller cross-section than that of perpendicular to the short axis. Consequently, the efficiency factors of absorption $Q_{abs,\parallel}$ and $Q_{abs,\perp}$ can be differentiated. In Fig. 3, $Q_{abs,\parallel}$ and $Q_{abs,\perp}$ are shown for compact silicate spheroids of shape 1-1.5-1 as well as the averaged absorption $\overline{Q}_{abs} = 0.5\left(Q_{abs,\parallel} + Q_{abs,\perp}\right)$ for different porosities. One can see that the absorption perpendicular to the short axis is larger than that of parallel to the short axis for wavelengths $\lambda > 2\pi a_{eff}$. Furthermore, the absorption efficiency increases with increasing porosity for wavelengths $\lambda \lesssim 2a_{eff}$ or $\lambda \gtrsim 10a_{eff}$, while the order is reversed at intermediate wavelengths. We note that we compare grains of different porosity but with the same effective radius a_{eff}. Therefore, the grains have the same mass but a
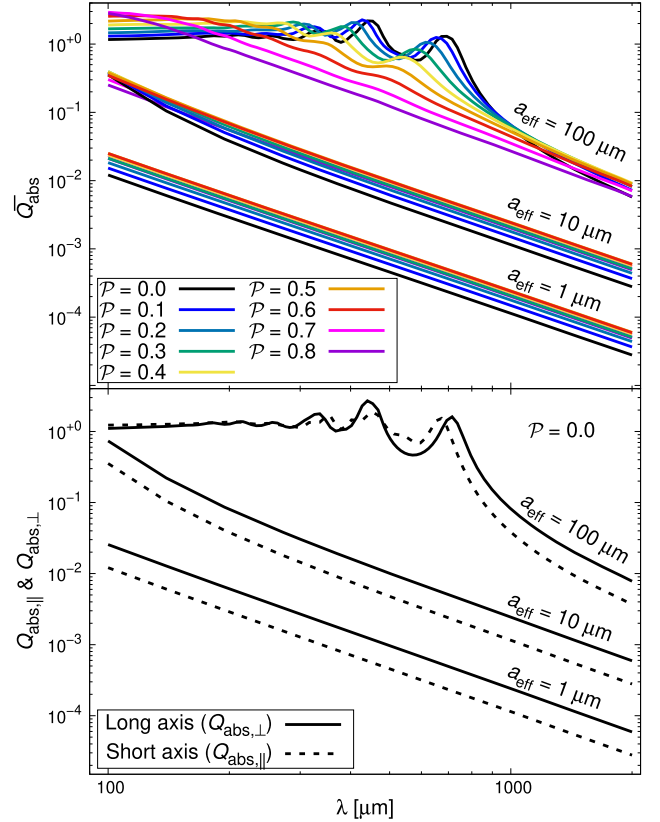

Figure 3. Absorption efficiency as a function of wavelength λ. The dust grain is prolate (1-1.5-1), composed of astronomical silicate and has an effective dust radius of $a_{eff} = 1$, 10, and 100 µm, respectively. *Top:* Averaged absorption $\overline{Q}_{abs}$ as a function of porosity $\mathcal{P}$. *Bottom:* Absorption of the long and short axes for compact spheroids ($\mathcal{P} = 0.0$).

different spatial extension (V_{total}). However, we show in Appendix A that the dependence of $\overline{Q}_{abs}$ on the porosity is still present if grains with same spatial extension but different mass are compared.

Since the absorption is different for the long and the short axes, the radiation gets polarized. Moreover, the efficiency factor of emission is equal to that of absorption ($Q_{emi} = Q_{abs}$), and radiation emitted by elongated dust grains is polarized in the same way. The degree of intrinsic polarization by emission from elongated dust grains is then (Cho & Lazarian 2007)

$$P_{emi} = \frac{Q_{abs,\perp} - Q_{abs,\parallel}}{Q_{abs,\perp} + Q_{abs,\parallel}}. \tag{3}$$

The degree of intrinsic polarization of prolate silicate grains (1-1.5-1) is shown in Fig. 4 (*top row*) as a function of wavelength λ, porosity $\mathcal{P}$, and effective grain size a_{eff}. For the small- and medium-sized grains ($a_{eff} = 1$ and 10 µm), we can see the following:

Porosity: The degree of intrinsic polarization P_{emi} is decreasing with increasing porosity $\mathcal{P}$ for all particle shapes. This is surprising, as one would expect intuitively an increase of polarization with increasing porosity. Moreover, the polarization by scattering of porous grains increases with porosity in the optical wavelength range (Kirchschlager & Wolf 2014).

Wavelength: In the far-infrared to millimetre wavelength range, the intrinsic polarization P_{emi} is nearly independent of the wavelength λ. Only for $a_{eff} = 10$ µm and at wavelengths $\lambda \sim 100$ µm, a weak wavelength dependence is visible for the polarization.
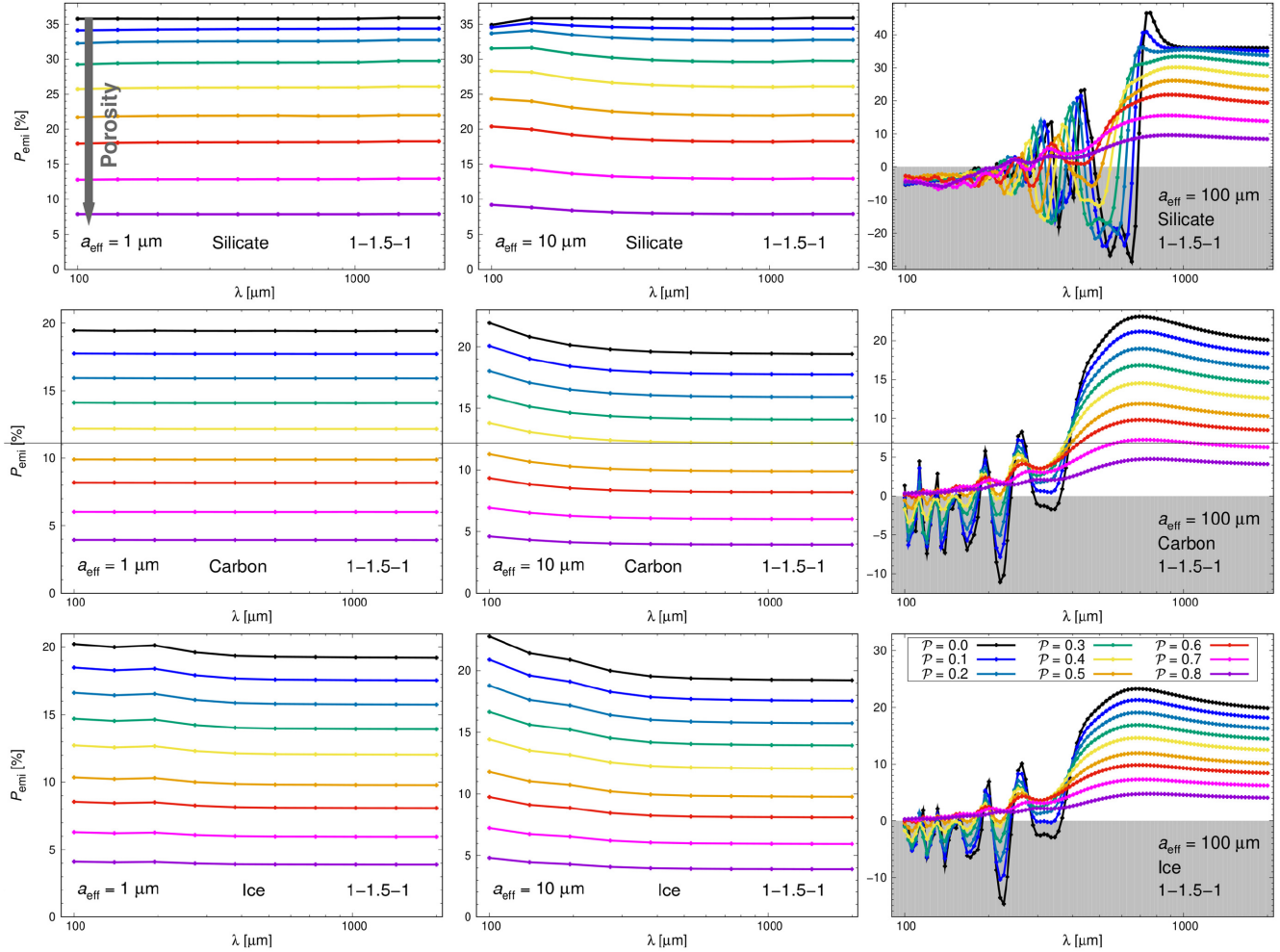
Figure 4. Intrinsic polarization $P_{\rm emi}$ as a function of wavelength λ, porosity $\mathcal{P}$, and effective grain radii $a_{\rm eff} = 1$, 10, and 100 μm for prolate (1-1.5-1) dust grains. The dust material is astronomical silicate (*top* row), carbon (*middle*), and ice (*bottom*). The grey-coloured regions emphasize negative polarizations that cause a 90 deg-flip of the polarization direction.

Axis ratio: The intrinsic polarization $P_{\rm emi}$ increases with increasing asphericity of the particles (Fig. 5), as the ratio of long to short semi-axis $\frac{c}{b}$ determines the absorption cross-sections $Q_{\rm abs, \perp}$ and $Q_{\rm abs, \parallel}$. The longer prolate grains or the flatter oblate grains, the larger the polarization.

Prolate/oblate: The intrinsic polarization $P_{\rm emi}$ is slightly higher for oblate compared to prolate grains of the same axis ratio $\frac{c}{b}$; however, the difference is for most wavelengths and grain sizes below 2 per cent (Fig. 5). Therefore, the ratio of long to short semi-axis $\frac{c}{b}$ and the porosity $\mathcal{P}$ are the only parameters of the particle morphology that have significant influence on the intrinsic polarization $P_{\rm emi}$.

For the $a_{\rm eff} = 100$ μm grains (*right* columns in Figs 4 and 5), the polarization degree shows a strong dependence on the wavelength. Oscillations occur as a result of enhanced interferences due to multiple reflection of the electromagnetic wave within the grain at $\lambda \sim 2\pi a_{\rm eff}$ (van de Hulst 1981). The oscillations enable even 'negative polarization' that causes a flip of the polarization direction, similar to the polarization reversal by scattering in the optical regime (e.g. Kirchschlager & Wolf 2014). While the polarization vector is parallel to the long grain axis (for both prolate and oblate grains) for $\lambda \gtrsim 2\pi a_{\rm eff}$, the polarization direction is perpendicular to the long

axis for smaller wavelengths. The amplitudes of the oscillations are slightly stronger for oblate grains compared to prolate grains but occur at similar wavelengths. Furthermore, the amplitudes of the oscillations decrease with increasing porosity as the voids hamper multiple reflection. For $\lambda \lesssim 2 a_{\rm eff}$ or $\lambda \gtrsim 10 a_{\rm eff}$, the wavelength dependence vanishes completely. Although the oscillations complicate the trends observed for the small and medium sized grains, the curves for the $a_{\rm eff} = 100$ μm grains are also ordered in a way that the amount of intrinsic polarization is decreasing with increasing porosity and increasing with the ratio of long to short axis $\frac{c}{b}$, at least for wavelengths $\lambda \gtrsim 3 a_{\rm eff}$.

Regarding the grain size, three cases can be differentiated: for $\lambda \gtrsim 10 a_{\rm eff}$ (Rayleigh regime), the effective radius $a_{\rm eff}$ has no impact on the degree of polarization and $P_{\rm emi}$ is constant. For $2 a_{\rm eff} \lesssim \lambda \lesssim 10 a_{\rm eff}$, interferences cause large oscillations in both absorption efficiency and intrinsic polarization. For $\lambda \lesssim 2 a_{\rm eff}$ (geometric optics regime), photons do not recognize the elongated shape. The absorption parallel to the short axis approaches that of the long axis, and the emission becomes unpolarized.

Fig. 4 shows also the degree of intrinsic polarization $P_{\rm emi}$ for grains composed of carbon (Jäger et al. 1998) and ice (Warren 1984; Reinert et al. 2015), respectively. The polarizations of these two materials are remarkably similar to each other. Compared to
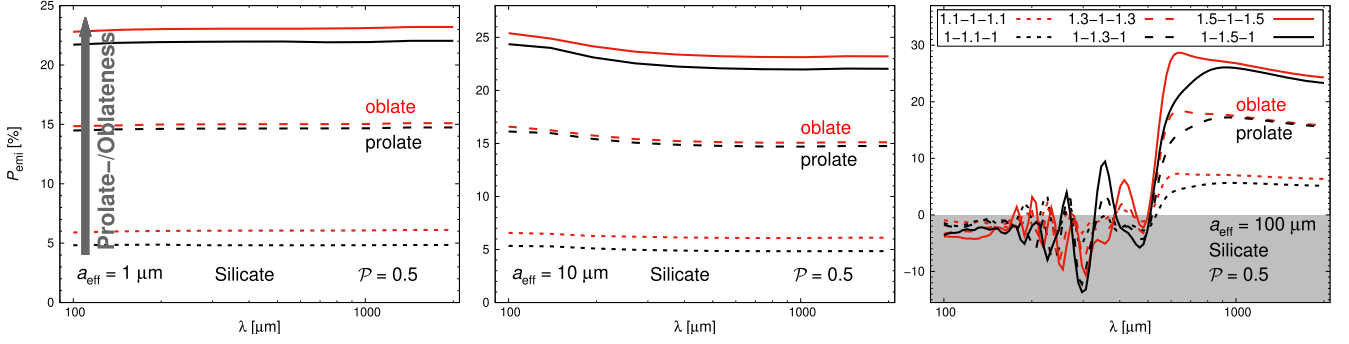
Figure 5. Intrinsic polarization P_{emi} as a function of prolate- (black) or oblateness (red) for elongated silicate grains with axis ratio $\frac{c}{b} = 1.1$, 1.3, or 1.5 (dotted, dashed, solid lines). The porosity is fixed to $\mathcal{P} = 0.5$ and the material is astronomical silicate.

astronomical silicate, P_{emi} is ~ 15 per cent lower for carbon and ice, the oscillations occur at shorter wavelengths ($\lambda < 4a_{\mathrm{eff}}$) and at the same wavelengths for different porosities. Despite that, all trends observed for the intrinsic polarization of astronomical silicate are also visible for carbon and ice.

To verify our results obtained with DDSCAT (based on DDA), we further performed simulations based on the T-Matrix method (TMM). We used the code MSTM (Multiple Sphere T-Matrix; Mackowski & Mishchenko 1996) to calculate the absorption and hence the intrinsic polarization for a configuration of multiple spheres arranged to approximate an elongated (porous) dust grain. The intrinsic polarization obtained with TMM (Fig. B1) shows the same trends as that obtained with DDA. For details, we refer to Appendix B.

3.2 Polarized emission in a protoplanetary disc

Dust grains in protoplanetary discs occur in different sizes, and the resulting polarization by emission will be composed of the contribution of each grain size. For an optically thin disc in which all dust grains are perfectly aligned, the degree of intrinsic polarization is estimated by (cf. Cho & Lazarian 2007)

$$P_{\mathrm{emi,disk}}(\lambda) = \frac{\int_{a_{\min}}^{a_{\max}} \left[Q_{\mathrm{abs},\perp} - Q_{\mathrm{abs},\parallel} \right] a_{\mathrm{eff}}^2 n(a_{\mathrm{eff}}) \, \mathrm{d}a_{\mathrm{eff}}}{\int_{a_{\min}}^{a_{\max}} \left[Q_{\mathrm{abs},\perp} + Q_{\mathrm{abs},\parallel} \right] a_{\mathrm{eff}}^2 n(a_{\mathrm{eff}}) \, \mathrm{d}a_{\mathrm{eff}}}, \tag{4}$$

where $\mathrm{d}n(a_{\mathrm{eff}}) \sim a_{\mathrm{eff}}^{-\gamma} \, \mathrm{d}a_{\mathrm{eff}}$ is the number of grains in the interval $[a_{\mathrm{eff}}, a_{\mathrm{eff}} + \mathrm{d}a_{\mathrm{eff}}]$, $\gamma = 3.5$ is the grain size exponent, and $a_{\min}$ and $a_{\max}$ are the minimum and maximum radii of the grain size distribution, respectively. We set $a_{\min} = 5$ nm and $a_{\max} = 100 \, \mu\mathrm{m}$ and make use of the fact that the degree of intrinsic polarization is constant for $a_{\mathrm{eff}} \leq 0.1\lambda$. For $a_{\mathrm{eff}} > 0.1\lambda$, we interpolate the results obtained for $a_{\max} = 10$ and $100 \, \mu\mathrm{m}$. Considering 1000 grain sizes logarithmically equidistant distributed in the range between $a_{\min}$ and $a_{\max}$, we calculate $P_{\mathrm{emi, disc}}(\lambda)$ via equation (4).

The resulting polarization of the disc is presented in Fig. 6 for grains of shape 1-1.5-1 made of astronomical silicate. For simplicity, we only present the result for this particle, but note that the figures are qualitatively similar for the other grain shapes and dust materials.[3] While for single grains oscillations occur at wavelengths $\lambda \in [\sim 2 \, a_{\mathrm{eff}}, 10 \, a_{\mathrm{eff}}]$, these oscillations cancel out by the presence of different sizes.
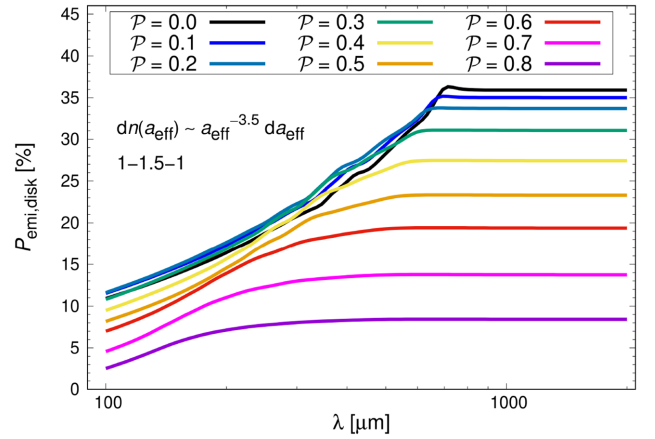

Figure 6. Degree of polarization by emission for an optically thin disc composed of 1-1.5-1 grains made of astronomical silicate, following a size distribution $\mathrm{d}n(a_{\mathrm{eff}}) \sim a_{\mathrm{eff}}^{-3.5} \mathrm{d}a_{\mathrm{eff}}$.

Following the trends of the single grains, the intrinsic polarization of the disc is decreasing with increasing porosity. We see that P_{emi} is linearly increasing with $\log(\lambda)$ before the curve reaches a 'knee' at a characteristic wavelength λ_{c}, and the polarization is getting constant for wavelengths $\lambda > \lambda_{\mathrm{c}}$. The reason for this break is the presence of grains that show oscillations for $\lambda < \lambda_{\mathrm{c}}$, resulting in cancellation or reduction of the intrinsic polarization, while all single grains show constant polarization for $\lambda > \lambda_{\mathrm{c}}$. As a consequence, when the maximum grain size $a_{\max}$ is varied we find a linear shift of the knee and the relation $\lambda_{\mathrm{c}} = 8 \, a_{\max}$ for compact silicate spheroids[4] ($\mathcal{P} = 0.0$; Fig. 7). For larger porosities, the knee is less pronounced and shifted to shorter wavelengths (Fig. 8).

We also varied the minimum grain size $a_{\min}$ for a fixed maximum grain size $a_{\max}$. While the values for the characteristic wavelength λ_{c} are unaffected, the slope at small wavelengths is steeper for larger $a_{\min}$ and shows oscillations, a consequence of the missing smoothing effect of the removed small particles. On the other hand, a reduction of the minimum grain size to lower values results in a flatter and smoother slope. Similar to that, we varied the grain size exponent γ between 3 and 4 and find that values close to 3 (reduced number of small grains) cause larger oscillations, while $\gamma \sim 4$ gives

---

[3]The intrinsic polarization data for grain size distributions of other grain shapes and dust materials are online available as supplementary material.

[4]For the standard MRN distribution (Mathis, Rumpl & Nordsieck 1977) with $a_{\max} = 0.25 \, \mu\mathrm{m}$, we expect a constant intrinsic polarization for all wavelengths in the interval $\lambda \in [100 \, \mu\mathrm{m}, 2000 \, \mu\mathrm{m}]$.
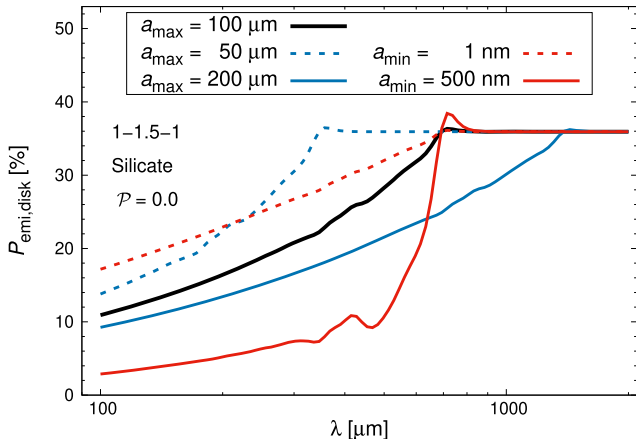
Figure 7. Influence of maximum (blue) or minimum (red) grain size on the degree of intrinsic polarization for silicate grains: the thick, black line represents the reference case ($a_{min} = 5$ nm; $a_{max} = 100$ μm), dotted lines are the polarization for a reduced minimum/maximum grain size, and the thin, solid lines are for an increased minimum/maximum grain size.
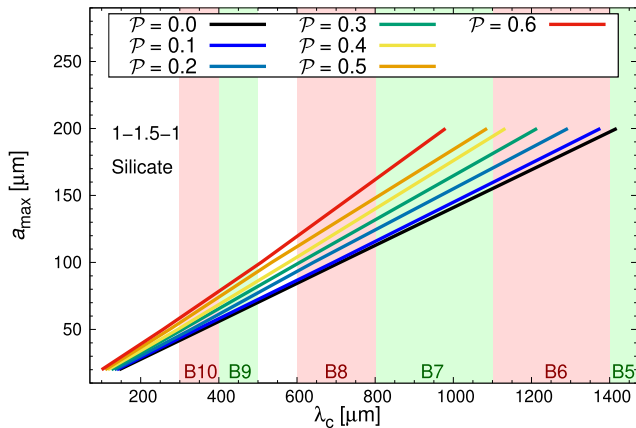

Figure 8. Relation between the maximum grain radius a_{max} of the grain size distribution and the characteristic wavelength λ_c at which the break from linearly increasing to constant polarization $P_{emi,disc}$ occurs (knee). The coloured shaded regions represent the ALMA wavebands B5 to B10.

a flatter and smoother slope too. In both cases, varying a_{min} and γ does not change the characteristic wavelength λ_c, which is only a function of the maximum grain size and porosity. Moreover, the characteristic wavelength is unaffected by the axis ratio $\frac{c}{b}$ while it shifted to by a factor of 2 shorter wavelengths for carbon or ice composition.

We note that the presented polarization values are derived under the assumption of perfectly aligned dust grains. However, grains in protoplanetary discs will be only partially aligned, and some parts of the disc will be optically thick, both reducing the amount of intrinsic polarization (e.g. Cho & Lazarian 2007; Bertrang et al. 2017; Bertrang & Wolf 2017).

4 IMPLICATIONS FOR POLARIZATION OBSERVATIONS

We have seen in Section 3 that the characteristic wavelength λ_c only depends on the maximum grain size and the porosity but not on further grain size properties such as the axis ratio $\frac{c}{b}$, the minimum

grain size or the grain size exponent. As the maximum grain size can be derived from other observation techniques, e.g. from the (sub)millimetre slope of the spectral energy distribution of the total intensity (Beckwith et al. 1990) or from the wavelength at which the scattering polarization peaks due to self-scattering[5] (Kataoka et al. 2015), determining the characteristic wavelength offers a tool to derive the grain porosity in a protoplanetary disc. Then, surveying the wavelength dependence on the integrated intrinsic polarization in the far-infrared and millimetre wavelength range provides insight in the internal structure of the disc's building blocks. On the other hand, knowing the grain porosity from other techniques, e.g. from the observation of the flipping of the polarization direction by scattering at optical wavelengths (Daniel 1980; Kirschlager & Wolf 2014), or from the dust opacity index at (sub)millimetre wavelengths (Kataoka et al. 2014), the intrinsic polarization can be used to derive or verify the maximum grain size in the disc.

Ohashi et al. (2018) detected polarization fractions at wavelengths $\lambda = 0.87$ mm as high as ~ 15 per cent in regions of the protoplanetary disc HD 142527. They interpreted this polarization signal most likely due to grain alignment with magnetic fields and thus as intrinsic polarization. Since we find that intrinsic polarization is decreasing with increasing porosity, the detection of Ohashi et al. (2018) sets an upper limit for the grain porosity in HD 142527. For a size distribution of silicate grains with maximum radii $a_{max} = 100$ μm and axis ratio $\frac{c}{b} = 1.5$ (Fig. 6), the intrinsic polarizations can take values up to 15 per cent only for grains with porosities lower than $\mathcal{P} = 0.7$. The maximum porosity is even lower for carbon or ice grains, for grains with lower axis ratio $\frac{c}{b}$, or larger maximum grain sizes. For silicate grains with $\frac{c}{b} = 1.3$ and $a_{max} = 100$ μm, only grain porosities up to $\mathcal{P} \leq 0.5$ are able to explain such high polarization fractions, while the intrinsic polarization from $\frac{c}{b} = 1.1$ spheroids is even too low for compact spheroids. Furthermore, if we assume that the grains are not perfectly aligned, the integrated polarization signal is weaker pronounced, further decreasing the maximum porosity. The only possibility for the presence of larger grain porosities to be consistent with high polarization fractions is to significantly increase the grain's axis ratio $\frac{c}{b}$.

Observations of several other discs show polarization fractions in the order of ~ 1 per cent and the most common explanations are self-scattering or intrinsic polarization combined with depolarization effects in optically thick regimes (e.g. Kataoka et al. 2017; Girart et al. 2018; Sadavoy et al. 2018; Dent et al. 2019). Consequently, the observed polarization is not pure intrinsic polarization in these discs, the determination of the characteristic wavelength λ_c is not suitable to constrain grain porosity, and we are not able to completely rule out highly porous dust grains for these discs.

Finally, we note that the change of the polarization sign at certain wavelengths (Figs 6 and 7) comes along with a drop of the polarization, passes a null level and then rebuilds the polarized

---

[5]We would like to emphasize that the current model for self-scattering is based on perfectly spherical dust grains (Kataoka et al. 2015). This simplification of grain geometry, while being accurate for the description of scattering of the stellar light, is not applicable for description of scattering of the thermal dust emission. While the stellar light is intrinsically (almost perfectly) unpolarized, the thermal dust emission is intrinsically polarized. The intrinsic polarization state of the emission depends on the grain geometry and, thus, changes the polarization state after the scattering event (see Kirschlager & Bertrang, in preparation). Therefore, it is advisable to take predictions of dust grain sizes based on current self-scattering models with caution.

intensity, where the new orientation is flipped by 90 deg. This might explain the observed and still unexplained multiwavelength pattern in HL Tau, especially in waveband 3 (Stephens et al. 2017). Future observations of the linearly polarized gas emission will test this explanation.

5 CONCLUSIONS

We have calculated the intrinsic polarization P_{emi} for elongated porous dust grains in the far-infrared to millimetre wavelength range. Our results depend on the grain's effective radius a_{eff} as the following:

(i) The amount of intrinsic polarization P_{emi} is decreasing with increasing porosity $\mathcal{P}$ for all particle shapes, an unexpected result as one would expect an increase of polarization with increasing porosity. This result includes $100\,\mu$m grains, though they are impaired by the present oscillations in the corresponding wavelength range ($2\,a_{eff} \lesssim \lambda \lesssim 10\,a_{eff}$).

(ii) The intrinsic polarization P_{emi} of silicate grains is nearly independent of the wavelength λ for $\lambda \gtrsim 10\,a_{eff}$. For $2\,a_{eff} \lesssim \lambda \lesssim 10\,a_{eff}$, oscillations occur for the absorption efficiency and the intrinsic polarization. These oscillations are a result of enhanced interferences due to multiple reflection of the electromagnetic wave within the grain and enable even 'negative polarization' that implies a reversal of the polarization direction. For $\lambda \lesssim 2\,a_{eff}$ (geometric optics regime), the emission becomes unpolarized.

(iii) The intrinsic polarization P_{emi} increases with increasing asphericity of the particles, defined by the ratio of long to short semi-axis $\frac{c}{b}$. The longer prolate grains or the flatter oblate grains, the larger the polarization.

(iv) Whether the grains are prolate or oblate has only a minor impact on the intrinsic polarization P_{emi}. The amplitudes of the oscillations are slightly stronger for oblate grains compared to prolate grains but occur at similar wavelengths. Therefore, the ratio of long to short semi-axis $\frac{c}{b}$ and the porosity $\mathcal{P}$ are the only parameters of the particle morphology that have significant influence on the polarization P_{emi}.

(v) Besides grains made of astronomical silicate, the trends exist for carbon as well as icy grains though the wavelength dependence is slightly different.

We summarize for a grain size distribution in a protoplanetary disc:

(i) Similar to the single grains, the intrinsic polarization of the disc is decreasing with increasing porosity. $P_{emi,\,disc}$ is linearly increasing with $\log(\lambda)$ for $\lambda < \lambda_c$ and constant for larger wavelengths.

(ii) The characteristic wavelength λ_c is proportional to the maximum radius of the grain size distribution. For larger porosities, the characteristic wavelength λ_c is shifted to shorter wavelengths.

(iii) The minimum grain size a_{min} and the grain size exponent γ have an impact on the steepness and the smoothness of the slope of the intrinsic polarization for wavelengths $\lambda < \lambda_c$, but not on the characteristic wavelength λ_c.

(iv) Surveying the wavelength dependence of the integrated intrinsic polarization in the far-infrared and millimetre wavelength range provides a tool to derive the grain porosity or maximum grain size in a protoplanetary disc.

(v) Observed polarization fractions in optically thin regions of protoplanetary discs (e.g. for HD 142527) set upper limits for the present grain porosities of up to ~ 70 per cent, rejecting highly porous (fluffy) grains unless the grain's axis ratio is significantly

larger than 1.5. Intrinsic polarization data of several grain shapes and dust materials are online available as supplementary material and allow the interpretation of future polarization observations.

REFERENCES

Beckwith S. V. W., Sargent A. I., Chini R. S., Guesten R., 1990, AJ, 99, 924
Bertrang G. H.-M., Wolf S., 2017, MNRAS, 469, 2869
Bertrang G. H.-M., Flock M., Wolf S., 2017, MNRAS, 464, L61
Blum J., Wurm G., 2008, ARA&A, 46, 21
Cho J., Lazarian A., 2007, J. Korean Astron. Soc., 40, 113
Cox E. G., Harris R. J., Looney L. W., Li Z.-Y., Yang H., Tobin J. J., Stephens I., 2018, ApJ, 855, 92
Daniel J.-Y., 1980, A&A, 87, 204
Dent W. R. F., Pinte C., Cortes P. C., Ménard F., Hales A., Fomalont E., de Gregorio-Monsalvo I., 2019, MNRAS, 482, L29
Dominik C., Tielens A. G. G. M., 1997, ApJ, 480, 647
Draine B. T., 2000, The Discrete Dipole Approximation for Light Scattering by Irregular Targets, Academic Press, San Diego, p. 131
Draine B. T., 2003a, ApJ, 598, 1017
Draine B. T., 2003b, ApJ, 598, 1026
Draine B. T., Flatau P. J., 1994, J. Opt. Soc. Am. A, 11, 1491
Draine B. T., Flatau P. J., 2010, preprint (arXiv:1002.1505)
Draine B. T., Goodman J., 1993, ApJ, 405, 685
Draine B. T., Weingartner J. C., 1996, ApJ, 470, 551
Draine B. T., Weingartner J. C., 1997, ApJ, 480, 633
Fulle M. et al., 2015, ApJ, 802, L12
Girart J. M. et al., 2018, ApJ, 856, L27
Gold T., 1952, MNRAS, 112, 215
Harrison R. E. et al., 2019, MNRAS, 877, L2
Harris R. J. et al., 2018, ApJ, 861, 91
Hull C. L. H. et al., 2018, ApJ, 860, 82
Jäger C., Mutschke H., Henning T., 1998, A&A, 332, 291
Kataoka A. et al., 2015, ApJ, 809, 78
Kataoka A. et al., 2016, ApJ, 831, L12
Kataoka A., Okuzumi S., Tanaka H., Nomura H., 2014, A&A, 568, A42
Kataoka A., Tsukagoshi T., Pohl A., Muto T., Nagai H., Stephens I. W., Tomisaka K., Momose M., 2017, ApJ, 844, L5
Kirchschlager F., Wolf S., 2013, A&A, 552, A54
Kirchschlager F., Wolf S., 2014, A&A, 568, A103
Kothe S., Blum J., Weidling R., Güttler C., 2013, Icarus, 225, 75
Langevin Y. et al., 2016, Icarus, 271, 76
Lazarian A., Hoang T., 2007, MNRAS, 378, 910
Lee C.-F., Li Z.-Y., Ching T.-C., Lai S.-P., Yang H., 2018, ApJ, 854, 56
Mackowski D. W., Mishchenko M. I., 1996, J. Opt. Soc. Am. A, 13, 2266
Mannel T., Bentley M. S., Schmied R., Jeszenszky H., Levasseur-Regourd A. C., Romstedt J., Torkar K., 2016, MNRAS, 462, S304
Mathis J. S., Rumpl W., Nordsieck K. H., 1977, ApJ, 217, 425
Milli J. et al., 2019, A&A, 626, A54
Mishchenko M. I., Travis L. D., Mackowski D. W., 1996, J. Quant. Spec. Radiat. Transf., 55, 535
Ohashi S. et al., 2018, ApJ, 864, 81
Ormel C. W., Spaans M., Tielens A. G. G. M., 2007, A&A, 461, 215
Pinte C. et al., 2008, A&A, 489, 633
Purcell E. M., Pennypacker C. R., 1973, ApJ, 186, 705
Rao R., Girart J. M., Lai S.-P., Marrone D. P., 2014, ApJ, 780, L6
Reinert C., Mutschke H., Krivov A. V., Löhne T., Mohr P., 2015, A&A, 573, A29
Sadavoy S. I. et al., 2018, ApJ, 859, 165

Segura-Cox D. M., Looney L. W., Stephens I. W., Fernández-López M., Kwon W., Tobin J. J., Li Z.-Y., Crutcher R., 2015, ApJ, 798, L2

Stephens I. W. et al., 2014, Nature, 514, 597

Stephens I. W. et al., 2017, ApJ, 851, 55

Takahashi S., Machida M. N., Tomisaka K., Ho P. T. P., Fomalont E. B., Nakanishi K., Girart J. M., 2019, ApJ, 872, 70

Tamura M., Hough J. H., Greaves J. S., Morino J.-I., Chrysostomou A., Holland W. S., Momose M., 1999, ApJ, 525, 832

Tazaki R., Tanaka H., 2018, ApJ, 860, 79

Tazaki R., Lazarian A., Nomura H., 2017, ApJ, 839, 56

van de Hulst H. C., 1981, Light Scattering by Small Particles,, Dover, New York

Warren S. G., 1984, Appl. Opt., 23, 1206

Ysard N., Jones A. P., Demyk K., Boutéraon T., Koehler M., 2018, A&A, 617, A124

SUPPORTING INFORMATION

Supplementary data are available at *MNRAS* online.

Please note: Oxford University Press is not responsible for the content or functionality of any supporting materials sup-

plied by the authors. Any queries (other than missing material) should be directed to the corresponding author for the article.

APPENDIX A: ABSORPTION EFFICIENCY OF POROUS DUST GRAINS OF CONSTANT SPATIAL EXTENSION

In Section 3, we compare grains with fixed effective radius a_{eff} but different spatial extension. Here, we want to emphasize that the presented effects are not caused by comparing grains of different spatial extension. Therefore, we fix the radius of the encompassing spheroid to $a_{\mathrm{eff}}/(1-\mathcal{P})^{1/3} = 1$, 10, and 100 μm, respectively, and determine the intrinsic polarization P_{emi} for prolate grains (1-1.5-1; astronomical silicate; Fig. A1). We can see a similar behaviour of P_{emi} compared to the case of a fixed effective radius a_{eff} (Fig. 4; *top* row), though the oscillations are shifted by a factor of $(1-\mathcal{P})^{1/3}$ to shorter wavelengths.
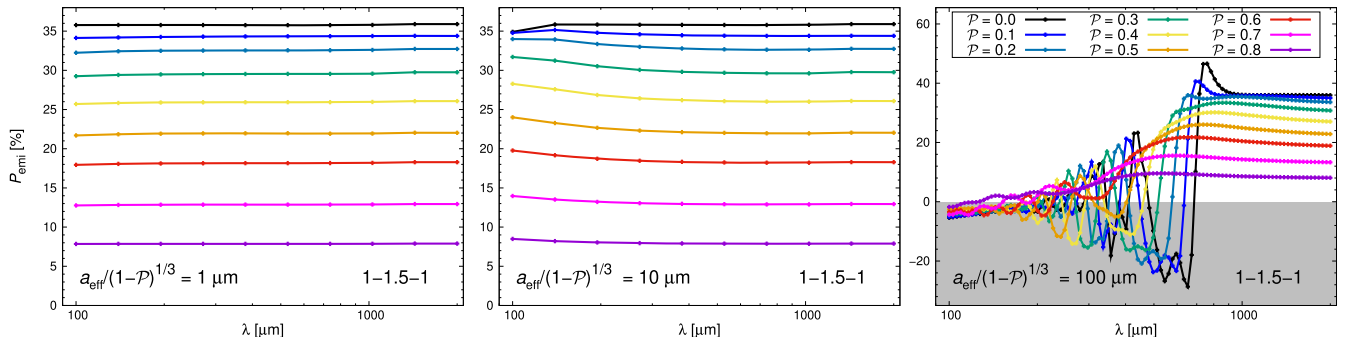

Figure A1. Intrinsic polarization for elongated porous silicates with fixed spatial extension, given by $a_{\mathrm{eff}}/(1-\mathcal{P})^{1/3}$ (cf. Fig. 4; *top* row).
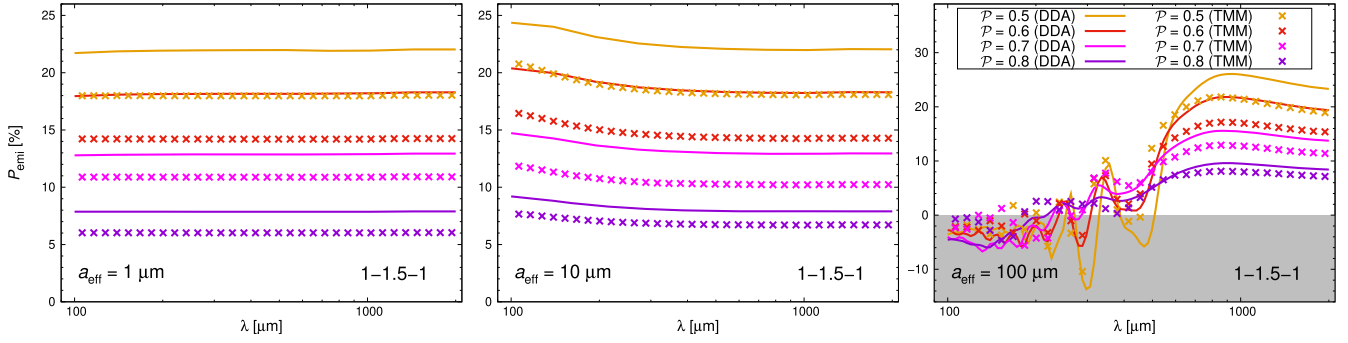
Figure B1. Comparison of results obtained with DDA (solid lines) and TMM (crosses) for the intrinsic polarization P_{emi} as a function of wavelength λ. The silicate grains are prolate (1:1.5:1) and have effective dust radii of $a_{eff} = 1$, 10, and 100 μm, respectively, and a porosity $\mathcal{P}$ between 0.5 and 0.8.
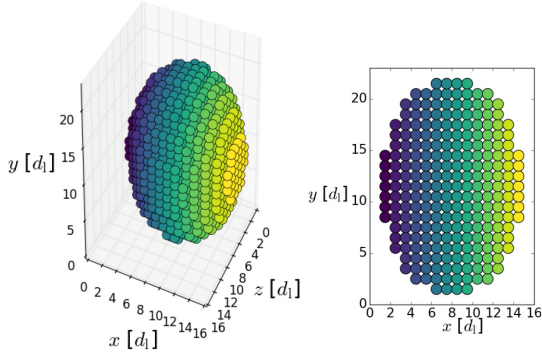

Figure B2. Morphology of an elongated porous dust grain (1-1.5-1) composed of 2204 equally sized spheres in a simple packing of spheres (*left*). The inherent porosity (given by the voids between the spheres) is $\mathcal{P} = 0.4764$. A single-layer of spherical monomers through the grain centre is shown (*right*).

APPENDIX B: COMPARISON BETWEEN TMM AND DDA

In order to verify our results, we consider a second calculation method that is unattached from calculations based on the DDA. We use the code MSTM[6] (version 3.0) that applies the TMM for an agglomeration of spherical monomers (Mackowski & Mishchenko 1996). Solving for the exact Mie solution of the single spheres,

the optical properties of the agglomerate are determined on the superposition principle (Mishchenko, Travis & Mackowski 1996).

The three-dimensional particle shape of the elongated porous particle is replaced by a corresponding spatial distribution of N_s spherical monomers. Because of the spherical geometry of the these monomers, stacking of them results in empty voids between the spheres that causes an inherent porosity of the agglomerate. For the sake of simplicity, we place N_s equally sized spheres on a cubic grid (sc-lattice),[7] forming an inherent porosity of $\mathcal{P} \approx 0.4764$. Lower porosities are not considered.

We set $N_s = 2204$ to form a prolate grain with shape 1-1.5-1 and porosity $\mathcal{P} \approx 0.4764$ (Fig. B2). For larger numbers N_s, TMM computations become time-consuming. We then randomly remove 99 (520; 941; 1362) spherical monomers to generate a spheroidal grain with porosity $\mathcal{P} = 0.5$ (0.6; 0.7; 0.8). These four particles are used to calculate the intrinsic polarization P_{emi} using TMM and to compare it with the corresponding results obtained with DDA (Fig. B1). We note that the amounts of P_{emi} derived from TMM calculations are slightly smaller than that derived from DDA calculations for all grain sizes. However, considering the fact that the calculations have been conducted with totally different approximation methods, the presented results show a good agreement. Moreover, the simulations based on TMM confirm that the intrinsic polarization of elongated dust grains is decreasing with increasing grain porosity.

---

[7]We note that even the close-packing of equal spheres (fcc- or hcp-lattice) has an inherent porosity of $\mathcal{P} \approx 0.2595$.

[6]http://www.eng.auburn.edu/~dmckwski/scatcodes/

This paper has been typeset from a TEX/LATEX file prepared by the author.